Engineering silicon nanocrystals: Theoretical study of the effect of codoping with boron and phosphorus

Federico Iori,[1] Elena Degoli,[2] Rita Magri,[1] Ivan Marri,[2] G. Cantele,[3] D. Ninno,[3] F. Trani,[3] O. Pulci,[4] and Stefano Ossicini[2]
[1]*CNISM-CNR and Dipartimento di Fisica, Università di Modena e Reggio Emilia, via Campi 213/A, I-41100 Modena, Italy*
[2]*CNR-INFM-S*[3] *and Dipartimento di Scienze e Metodi dell'Ingegneria, Università di Modena e Reggio Emilia, via Amendola 2 Padiglione Morselli, I-42100 Reggio Emilia, Italy*
[3]*CNR-INFM-Coherentia and Dipartimento di Scienze Fisiche, Università di Napoli "Federico II," Complesso Universitario Monte S. Angelo, Via Cintia, I-80126 Napoli, Italy*
[4]*European Theoretical Spectroscopy Facility (ETSF) and CNR-INFM, Dipartimento di Fisica, Università di Roma "Tor Vergata," Via della Ricerca Scientifica 1, I-00133 Roma, Italy*
(Received 23 January 2007; revised manuscript received 22 May 2007; published 1 August 2007)

We show that the optical and electronic properties of nanocrystalline silicon can be efficiently tuned using impurity doping. In particular, we give evidence, by means of *ab initio* calculations, that by properly controlling the doping with either one or two atomic species, a significant modification of both the absorption and the emission of light can be achieved. We have considered impurities, either boron or phosphorous (doping) or both (codoping), located at different substitutional sites of silicon nanocrystals with size ranging from 1.1 to 1.8 nm in diameter. We have found that the codoped nanocrystals have the lowest impurity formation energies when the two impurities occupy nearest neighbor sites near the surface. In addition, such systems present band-edge states localized on the impurities, giving rise to a redshift of the absorption thresholds with respect to that of undoped nanocrystals. Our detailed theoretical analysis shows that the creation of an electron-hole pair due to light absorption determines a geometry distortion that, in turn, results in a Stokes shift between adsorption and emission spectra. In order to give a deeper insight into this effect, in one case we have calculated the absorption and emission spectra beyond the single-particle approach, showing the important role played by many-body effects. The entire set of results we have collected in this work give a strong indication that with the doping it is possible to tune the optical properties of silicon nanocrystals.

DOI: 10.1103/PhysRevB.76.085302 PACS number(s): 78.67.Bf, 71.35.Cc, 73.20.Hb, 74.78.Na

I. INTRODUCTION

Bulk silicon is an indirect band-gap material emitting in the infrared region. Radiative lifetimes of excited carrier are very long, causing a predominant deexcitation via fast nonradiative recombinations. Moreover, silicon has a significant free carrier absorption and Auger recombination rate, which make the use of this material in optoelectronic applications very problematic.

During the past decade, several breakthroughs have increased the hopes of using nanostructured silicon as an optical active material.[1,2] The basic idea has been to take advantage of the reduced dimensionality of the nanocrystalline phase (1–5 nm in size), where quantum confinement, band folding, and surface effects play a crucial role.[1,3] Indeed, it has been found that Si nanocrystal band gap increases with decreasing size, with a luminescence external efficiency in excess of 23%.[1,3,4] Moreover, optical gain has already been demonstrated in a large variety of experimental conditions.[5–9] Nevertheless, Si nanocrystals (Si-nc) still have a memory of the indirect band gap of the bulk phase, and this is evidenced by the clearly observed structures related to momentum-conserving phonons.[1,10,11] This drawback can be circumvented by introducing isoelectronic impurities.[1,3] Indeed, in a series of recent very interesting papers, Fujii *et al.*[12–14] have proven the possibility of a detailed control of the Si-nc photoluminescence by the simultaneous doping with *n*- and *p*-type impurities. In particular, they have shown that a (B and P) codoped Si-nc always has a higher photoluminescence intensity than that of both a single (B or P) doped nanocrystal and an undoped nanocrystal. Besides, under resonant excitation condition, the codoped samples did not exhibit structures related to momentum-conserving phonons, suggesting that, in this case, the quasidirect optical transitions are predominant.[12–14]

From a theoretical point of view, investigations of impurities in silicon nanostructures are very few when compared to the large number of papers reporting calculations for pure, undoped systems; moreover, most of them are based on semiempirical approaches. A handful of first-principles studies has been devoted to quantum confinement effects in single-doped Si-nc.[15–18] These works have basically shown that (i) the Si-nc ionization energy is virtually size independent, (ii) the impurity formation energy is greater for smaller nanocrystals, and (iii) impurity segregation strongly affects the conductance properties of nanostructures.[15–18]

We have recently started a systematic study of the electronic and optical properties of codoped Si-nc. Our first results[19] show that codoped Si-nc undergoes a minor structural distortion around the impurities and that the formation energies are always smaller than those of the corresponding single-doped cases. Moreover, we have found that codoping reduces the band gap with respect to the undoped nanocrystals, showing the possibility of an impurity based engineering of the Si-nc optical properties.[19,20]

We report here a comprehensive theoretical study of the structural, electronic, and optical properties of B and P simultaneously doped Si nanocrystals using *ab initio* density

functional theory. The paper is organized as follows. Section II is focused on the description of the theoretical and computational methods; Sec. III is dedicated to the discussion of our results. The results will be presented and discussed in the following order: (i) structural properties (Sec. III A), (ii) formation energies (Sec. III B), and (iii) electronic (Sec. III C) and (iv) optical properties (Sec. III D) for all the considered Si nanocrystals. Concerning the optical properties, we discuss both absorption and emission spectra obtained within a single-particle approach (Sec. III D 1) and, in one case, with many-body methods considering self-energy corrections and the Bethe-Salpeter scheme (Sec. III D 2). Finally, in Sec. IV, we summarize our results.

II. COMPUTATIONAL METHODS

Our results are obtained within a plane-wave pseudopotential density functional theory (DFT) scheme, using the QUANTUM-ESPRESSO package.[21] The impurity states are calculated in an approximately spherical Si-nc, built by considering all the bulk Si atoms contained in a sphere (centered on a Si ion) with a diameter ranging from 1.1 nm ($Si_{35}H_{36}$) to 1.79 nm ($Si_{147}H_{100}$). The surface dangling bonds are saturated with hydrogens. Following the work of Fujii *et al.*,[12] we have located the B and P impurities in substitutional positions just below the nanocrystal surface. It is worth mentioning that this arrangement represents the most stable configuration, as confirmed by theoretical and experimental works.[19,22,23] Full relaxation with respect to the atomic positions has been allowed for both doped and undoped systems. All the DFT calculations are performed within the generalized gradient approximation using Vanderbilt ultrasoft[24] pseudopotentials for the determination of both the structural and electronic properties (see Secs. III A–III C), whereas norm-conserving pseudopotentials within the local density approximation (LDA) at the relaxed geometry have been used to evaluate the optical properties (see Sec. III D). This choice is due to the fact that although Vanderbilt ultrasoft pseudopotentials allow the treatment of several hundreds of atoms per unit cell in the atomic relaxation process, the removal of the norm-conservation condition is a well known problem for the calculation of the optical transition matrix elements.[25] Each nanocrystal has been placed in a large supercell in order to prevent interactions between the periodic replicas (about 6 Å of vacuum separates neighbor nanocrystals). Structural, electronic, and optical properties, as well as the impurity formation energies, are investigated as a function of the size and for several impurity positions within the Si-nc. Starting from the Si_nH_m nanocrystal,[26] the formation energy of the neutral B or/and P impurities can be defined as the energy needed to insert one B or/and one P atom within the nanocrystal after removing one or two Si atoms (transferred to the chemical reservoir, assumed to be bulk Si),[27]

$$E_f = E(\mathrm{Si}_{n-l-k}\mathrm{B}_k\mathrm{P}_l\mathrm{H}_m) - E(\mathrm{Si}_n\mathrm{H}_m) + (k+l)\mu_{\mathrm{Si}} - k\mu_{\mathrm{B}} - l\mu_{\mathrm{P}}, \tag{1}$$

where E is the total energy of the system, μ_{Si} the total energy per atom of bulk Si, and $\mu_{\mathrm{B(P)}}$ the total energy per atom of the impurity (we consider the total energy per atom in the tetragonal B_{50} crystal for B, as in Ref. 28, and the orthorhombic black phosphorus for P, as in Ref. 29). The integers k and l can be set to either 0 or 1. In particular, $k=1$ is the choice when a B impurity is present in the nanocrystal (0 otherwise) and $l=1$ for a P impurity (0 otherwise). With this prescription, Eq. (1) can be used for both the single doping case and the codoping case.

The calculations of the optical properties have been done both in the ground and first excited states, where the excited state corresponds to the electronic configuration in which the highest occupied single-particle state [highest occupied molecular orbital (HOMO)] contains a hole, while the lowest unoccupied single-particle state [lowest unoccupied molecular orbital (LUMO)] contains the corresponding electron.[30–33] It is worth pointing out that an undoped and relaxed Si-nc has T_d symmetry; in the presence of doping, this high symmetry is generally lost due to the presence of the impurity atoms. Moreover, because of the significant differences in the charge density of the ground and excited states, the actual atomic relaxations in the two cases are different.

The nanocrystal optical response is evaluated for both the ground and excited state relaxed geometries, computing the imaginary part of the dielectric function $[\epsilon_2(\omega)]$ through the Fermi golden rule. The emission spectra have been calculated using the excited state atomic positions and the ground state electronic configuration (more details can be found in Sec. III D 2). It should be noted that although $\epsilon_2(\omega)$ should only be used for calculating the nanocrystal absorption coefficient, it can also be used for getting a first approximation to the emission spectra simply because the emission can be viewed as the time reversal of the absorption.[34] In other words, once the relaxed atomic positions corresponding to a hole in the HOMO and an electron in the LUMO have been found, these atomic positions are used for the calculation of $\epsilon_2(\omega)$, whose main features are also those of the emission spectra. It is worth mentioning that the photoluminescence spectra can be derived using the well known Van Roosbroeck–Shockley[35] relation which, again, involves $\epsilon_2(\omega)$. However, such a calculation requires the knowledge of the electron and hole populations, at the working temperature, in the LUMO and HOMO states, respectively. The populations, in turn, depend on the actual dynamics in the excitation and emission processes, including the nonradiative electron-hole recombinations. In this work, we have not considered any particular dynamics, so that our emission spectra contains only the information related to both the transition energies and the oscillator strengths.

In the case of the $Si_{33}BPH_{36}$ codoped Si-nc, going beyond the single-particle approach, we have included the self-energy corrections by means of the GW approximation.[36] In a successive step, excitonic effects are included, solving the Bethe-Salpeter equation (BSE).[32] A further advantage of this procedure is that the inhomogeneity of the system is taken into account by properly including local field effects.[37] This approach, in which many-body effects are combined with a study of the structural distortion due to the impurity atoms in the excited state, allows a precise determination of the Stokes shift between absorption and emission spectra.[33]

TABLE I. Bond lengths (in Å) around the impurity sites for the undoped, single doped, and codoped $Si_{87}H_{76}$ nanocrystal (diameter: 1.50 nm). B and P impurities have been substitutionally located at subsurface positions (see Fig. 1). Si_s and Si_i refer to two surface and two inner Si atoms around this site, respectively.

Bond	$Si_{87}H_{76}$ (Å)	Bond	$Si_{86}BH_{76}$ (Å)	$Si_{86}PH_{76}$ (Å)	$Si_{85}BPH_{76}$ (Å)
Si-Si_s	2.355	B-Si_s	2.036		2.021
Si-Si_s	2.355	B-Si_s	2.036		2.021
Si-Si_i	2.363	B-Si_i	2.014		2.034
Si-Si_i	2.363	B-Si_i	2.014		2.034
Si-Si_s	2.355	P-Si_s		2.294	2.295
Si-Si_s	2.355	P-Si_s		2.294	2.295
Si-Si_i	2.363	P-Si_i		2.380	2.331
Si-Si_i	2.363	P-Si_i		2.380	2.331

III. RESULTS

This section collects all the results we have obtained in the study of the structural, electronic, and optical properties of boron and phosphorus codoped silicon nanocrystals. When possible, our outcomes are compared with available experimental results.

A. Structural properties

First of all, it is interesting to look at the change in the nanocrystal structure induced by the presence of the impurities. As outlined above, the B or/and P impurity atoms have always been located in substitutional sites in the Si shell just below the surface, these positions having previously been shown to be the most stable ones.[16] Initially, we have considered impurities located on opposite sides of the nanocrystals, thus, at the largest possible distance.

Table I gives the relaxed bond lengths around the impurities for $Si_{87}H_{76}$, whose structure is shown in Fig. 1. Comparing these bond lengths with those of the corresponding Si atoms in the undoped Si-nc, it is clear that some significant relaxation occurs around the impurities. In all the cases, the local structure has a C_{2v} symmetry, with two shorter and two longer Si-impurity bonds with respect to the two surface and two inner Si atoms. An interesting point is that the amount of relaxation around the impurity is directly related to the impurity valence. The most significant relaxation is found for the trivalent atom (B, 2.036 and 2.014 Å with respect to 2.355 and 2.363 Å) as compared with that of the pentavalent one (P, 2.294 and 2.380 Å with respect to 2.355 and 2.363 Å). Besides, it is interesting to note that in the codoped case, the differences among the four impurity-Si bond lengths are always smaller than the single-doped case (the Si-B bonds differ by about 1.08% in the single-doped case and by only 0.64% in the codoped case, whereas this variation in the case of P reduces from 3.61% to 1.54%). Thus, if carriers in the Si-nc are perfectly compensated by simultaneous *n*- and *p*-type dopings, an almost T_d configuration is recovered.

This tendency toward a T_d symmetry of codoped Si-nc is also obtained for smaller and larger nanocrystals, showing that these outcomes are independent of the Si-nc size. Anyway, a symmetry lowering with respect to $Si_{87}H_{76}$ is present due to the different neighborhood experienced by the impurities. It should, in fact, be noted that in the case of $Si_{35}H_{36}$ and $Si_{147}H_{100}$, the atoms in the first subsurface shell are bonded to three surface Si atoms and to one inner Si atom, while for $Si_{87}H_{76}$ they are bonded to two surface and two inner Si atoms. The impurity positions for the considered nanocrystals are shown in Figs. 1–3. Tables II and III give the structural modifications that occur around the impurities for $Si_{35}H_{36}$ and $Si_{147}H_{100}$, respectively. Even in these cases, the differences between the four Si-impurity bond lengths in going from the undoped to the single-doped to the codoped case first increase and then decrease.

Having stated that the amount of structural deformation remains unvaried as the nanocrystal size changes and having shown that this behavior is simply related to the codoping, we have devoted our attention on the effect of the presence of both impurities. We have looked, in particular, at what happens to the impurity-impurity distance when compared to

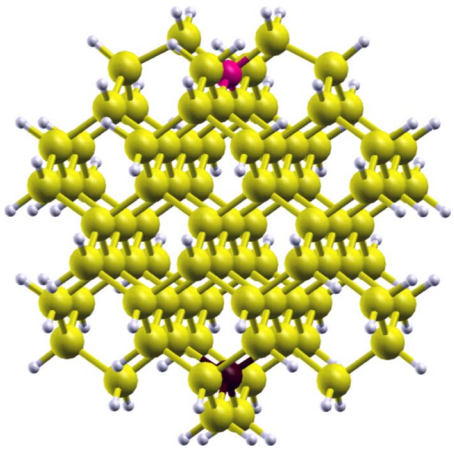

FIG. 1. (Color online) Relaxed structure of $Si_{85}BPH_{76}$ (d=1.50 nm). Yellow (gray) balls represent Si atoms, while the white (light gray) balls are the hydrogens used to saturate the dangling bonds. B (magenta, dark gray) and P (black) impurities have been located at subsurface position in substitutional sites on opposite sides of the nanocrystal. The relaxed impurity-impurity distance is D_{BP}=10.60 Å.

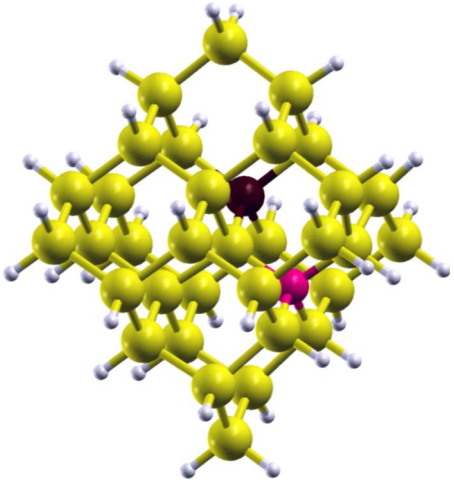

FIG. 2. (Color online) Relaxed structure of the $Si_{33}BPH_{36}$ codoped nanocrystal (d=1.10 nm). Yellow (gray) balls represent Si atoms, while the white (small gray) balls are the hydrogens used to saturate the dangling bonds. B (magenta, dark gray) and P (black) impurities have been located at subsurface position in substitutional sites on opposite sides of the nanocrystals. The relaxed impurity-impurity distance is D_{BP}=3.64 Å.

the corresponding Si-Si distance in the undoped nanocrystal. We have calculated these distances for $Si_{145}BPH_{100}$, keeping the B atom fixed in a subsurface position and moving the P atom through different substitutional sites along the first subsurface shell, as schematically shown in Fig. 4. We have moved the P atom from the position labeled II to the positions III, V-a, V-b, VI-a, VI-b, VIII-a, VIII-b, IX-a, IX-b, and X. Here, roman number refers simply to the positions evidenced in Fig. 4. For each configuration, we have calculated the B-P distance after a geometry relaxation and repeated the calculation for the corresponding Si-Si distance. The results are shown in Fig. 5, where, as a reference, we also show the

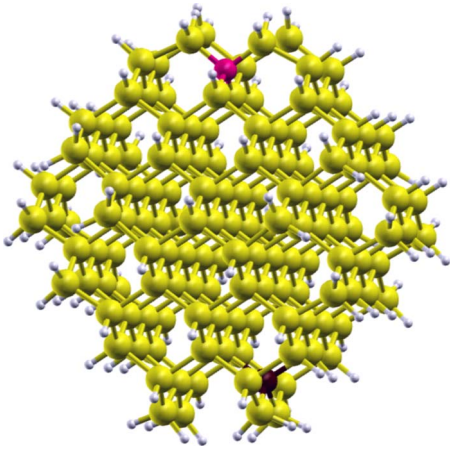

FIG. 3. (Color online) Relaxed structure of the $Si_{145}BPH_{100}$ codoped nanocrystal (diameter d=1.79 nm). Yellow (gray) balls represent Si atoms, while the white (small gray) balls are the hydrogens used to saturate the dangling bonds. B (magenta, dark gray) and P (black) impurities have been located at subsurface position in substitutional sites on opposite sides of the nanocrystals. The relaxed impurity-impurity distance is D_{BP}=13.59 Å.

corresponding distances in bulk silicon. By taking bulk silicon as a reference, values above the dashed line reflect an increase, whereas values below correspond to a reduction of the distances. It is seen that in all the cases considered, the distances are only weakly modified. Indeed, in going from the undoped nanocrystals (where the distances are almost the same as in bulk silicon) to the codoped ones, we note a very small shrinkage of the impurity-impurity distances. This shows, once again, that if carriers are perfectly compensated by simultaneous doping, the Si-nc does not really undergo a significant structural distortion, and this fact does not depend on the distance between the impurities.

B. Formation energy

The different structural deformations occurring in the single-doped and codoped nanocrystals around the impurity (see Tables I–III) have a deep influence on the stability of the analyzed systems. As stated in Sec. II, starting from Si_nH_m,[26] the formation energy of the neutral B or/and P impurities can be defined as the energy needed to insert one B or/and one P atom within the nanocrystal after removing one or two Si atoms.

In order to clarify which are the parameters that play an important role in the determination of the formation energy, we have performed a series of total energy calculations considering (i) single-doped and codoped nanocrystals, (ii) nanocrystals of different sizes, (iii) impurities located in different sites, and (iv) variable impurity-impurity distance within a nanocrystal.

In Fig. 6, we report the calculated formation energies of $Si_{35}H_{36}$ (diameter d=1.10 nm), $Si_{87}H_{76}$ (d=1.50 nm), and $Si_{147}H_{100}$ (d=1.79 nm). In the same figure, as a reference, we report also the single-doping formation energies. For the codoped case, B and P impurities have been placed as second neighbors. This choice corresponds to the nearest possible distance between two subsurface sites for both $Si_{33}BPH_{36}$ (see Fig. 2) and $Si_{145}BPH_{100}$ (see the position labeled II in Fig. 4). After a geometry relaxation, the distances between B and P impurities are D_{BP}=3.56 Å, D_{BP}=3.64 Å, and D_{BP} =3.68 Å for $Si_{33}BPH_{36}$, $Si_{85}BPH_{76}$, and $Si_{145}BPH_{100}$, respectively.

From Fig. 6, it is clear that the simultaneous B and P doping strongly reduces (of about 1 eV) the formation energy with respect to both B and P single-doped cases and that this reduction is similar for Si-nc of different sizes. Thus, while B or P single doping is very costly (in particular, the formation energy increases with decreasing nanocrystal size, in agreement with previous calculations[15,16]), the codoping is much easier and, as a good approximation, independent of the nanocrystal size. The important point here is that Si-nc can be more easily simultaneously doped than single doped; this is due to both the charge compensation and to the minor structural deformation.

It is interesting to look at the detailed dependence of the formation energy on the distance between the two impurities. In Fig. 7, we present the comparison between the formation energies of $Si_{85}H_{76}$ and $Si_{145}H_{100}$ with impurities placed at two different distances: (1) the previous considered second

TABLE II. Bond lengths (in Å) around the impurity sites for the undoped, doped, and codoped $Si_{35}H_{36}$ nanocrystal (d=1.10 nm). Substitutional B and P impurities are located at subsurface positions (see Fig. 2). Si_s and Si_i label, respectively, the three surface atoms and one inner Si atom around this site.

Bond	$Si_{35}H_{36}$ (Å)	Bond	$Si_{34}BH_{36}$ (Å)	$Si_{34}PH_{36}$ (Å)	$Si_{33}BPH_{36}$ (Å)
Si-Si_s	2.300	B-Si_s	2.093		2.035
Si-Si_s	2.300	B-Si_s	2.022		2.026
Si-Si_s	2.300	B-Si_s	2.022		2.026
Si-Si_i	2.361	B-Si_i	2.008		2.007
Si-Si_s	2.300	P-Si_s		2.366	2.303
Si-Si_s	2.300	P-Si_s		2.365	2.302
Si-Si_s	2.300	P-Si_s		2.364	2.297
Si-Si_i	2.361	P-Si_i		2.310	2.334

neighbors and (2) the largest possible impurity distance (D_{BP}=10.60 Å and D_{BP}=13.29 Å for $Si_{85}BPH_{76}$ and $Si_{145}BPH_{100}$, respectively, see Figs. 1 and 3). We note that when the impurity-impurity distance is reduced, the formation energy decreases by 0.2–0.3 eV, taking negative values. This fact demonstrates that a stronger interaction between impurities leads to a reduction in the formation energy, so that codoping becomes easier and more likely when the dopants are closer to each other. In the latter case, the reduction of the formation energy is almost independent of the nanocrystal size, as shown in Fig. 6.

In order to investigate in more detail the dependence of the formation energy on the impurity-impurity distance, we focus our attention on the codoped $Si_{145}BPH_{100}$, trying to trace a "formation energy path" by progressively increasing the B-P distance. In this calculation, we have kept the B atom frozen in a subsurface position while moving the P atom through different substitutional sites along the first subsurface shell, as schematically sketched in Fig. 4. The results of these calculations are shown in Fig. 8. Two interesting effects are evidenced in this figure. The first one is that the formation energy assumes a negative value when the impurities are placed at distances smaller than 10 Å, evolving toward positive values for larger distances. This change of sign can lead to the definition of a "critical impurity distance." Below such a threshold, the interaction between boron and phosphorus is strong and gives rise to a reduction of the formation energy. On the contrary, above this value, the interaction tends to be quenched, reducing the stability of the impurity complex.

These considerations are also supported by Fig. 9, where we report the values of the formation energy for three different nanocrystals in which the impurities are always located in the subsurface shells at different distances. As before, it is evident from this figure that the distance between impurities plays a fundamental role on the decrease of the formation energy. For each nanocrystal, the formation energy takes on negative values below a given distance. Moreover, the formation energy has a minimum value when the impurities are located at the minimum possible distance. Indeed, the impurity-impurity distance seems to play a major role with respect to the nanocrystal size, since the formation energy for similar impurity configurations is quite independent of the nanocrystal dimension. The small difference between $Si_{85}BPH_{76}$, $Si_{33}BPH_{36}$, and $Si_{145}BPH_{100}$ is due to the different neighborhoods experienced by the impurities in the three cases (see Tables I–III).

Another relevant point is the possibility of identifying two distinct trends for the formation energy (see Fig. 8) that can be related to the type of silicon cage surrounding the P dop-

TABLE III. Bond lengths (in Å) around impurity sites for the undoped, single doped, and codoped $Si_{147}H_{100}$ nanocrystal (d=1.79 nm). Substitutional B and P impurities are located at subsurface positions (see Fig. 3). Si_s and Si_i have the same meaning as in Table II.

Bond	$Si_{147}H_{100}$ (Å)	Bond	$Si_{146}BH_{100}$ (Å)	$Si_{146}PH_{100}$ (Å)	$Si_{145}BPH_{100}$ (Å)
Si-Si_s	2.356	B-Si_s	2.029		2.016
Si-Si_s	2.356	B-Si_s	2.029		2.016
Si-Si_s	2.356	B-Si_s	2.063		2.018
Si-Si_i	2.369	B-Si_i	2.009		2.022
Si-Si_s	2.356	P-Si_s		2.310	2.306
Si-Si_s	2.356	P-Si_s		2.310	2.306
Si-Si_s	2.356	P-Si_s		2.372	2.338
Si-Si_i	2.369	P-Si_i		2.321	2.321

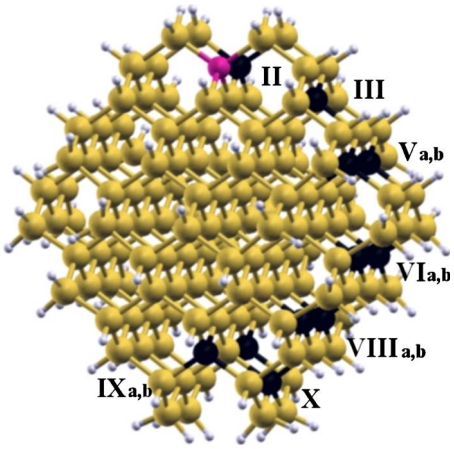

FIG. 4. (Color online) "Phosphorus impurity path" in $Si_{145}BPH_{100}$. Atoms have the same color as in Fig. 2. The P atom (black) has been moved to explore several substitutional sites (labeled by Roman numbers) from the position labeled by II to the positions III, V-a, V-b, VI-a, VI-b, VIII-a, VIII-b, IX-a, IX-b, and X. The B atom (magenta, dark gray) position is fixed.

ant site. One can group (dotted line) together the cases in which the P impurity is located in the positions labeled II, VI-b, and X with respect to the B impurity (see Fig. 4). In these positions, two of the surface Si atoms bonded to the P impurity present two passivating H atoms instead of one, a situation that dominates in all the other configurations. A different number of capping H atoms influences the formation energy.

C. Electronic properties

In this section, we will investigate the role of codoping on the electronic properties of Si-nc. As in the corresponding bulk system, the insertion of impurities tends to modify the electronic structure. We shall show that, by properly controlling the doping and the size, it is possible to modulate both the electronic structure and some optical features. In particular, we shall show how the electronic properties of the codoped nanocrystals depend on both the nanocrystal size and on the distance between the impurities. Some of the results will be discussed in terms of wave function localization around the impurity complex.

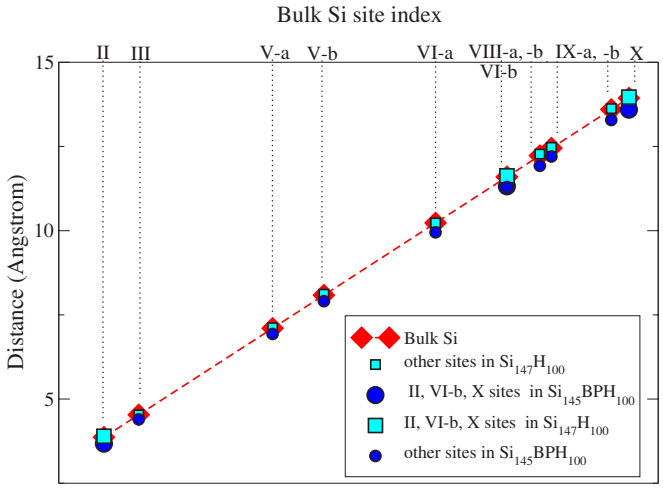

FIG. 5. (Color online) B-P substitutional site distances in $Si_{145}BPH_{100}$ (blue circles) and the corresponding Si-Si distances in the undoped $Si_{147}H_{100}$ nanocrystal (cyan squares) compared to the corresponding distances in bulk Si (black diamonds).

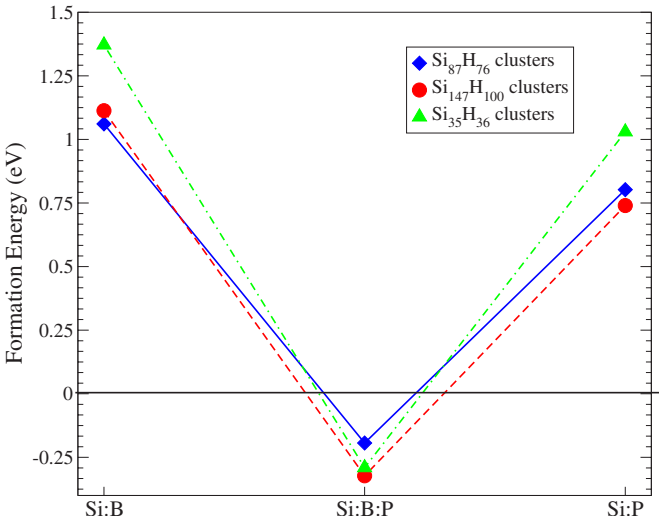

FIG. 6. (Color online) Formation energy for single-doped and codoped Si-nc. In the codoped nanocrystals, the impurities are placed as second neighbors in the first subsurface shell (see text). Green triangles are related to $Si_{35}H_{36}$, blue diamonds to $Si_{87}H_{76}$, and red circles to $Si_{147}H_{100}$ based nanocrystals. The lines are a guide for the eyes.

In the single-doped cases, we have already shown that the presence of either donor or acceptor states can considerably lower the energy gap (E_G, the HOMO-LUMO energy difference) of the undoped Si-nc,[16,19] defining in this case the en-

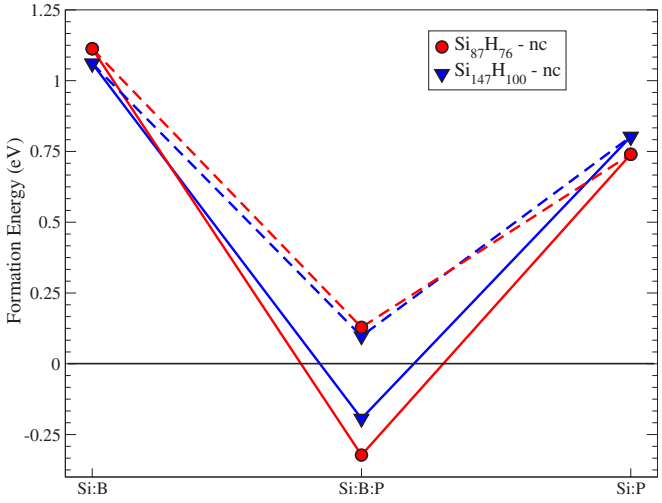

FIG. 7. (Color online) Formation energy of single-doped and codoped $Si_{87}H_{76}$ and $Si_{147}H_{100}$ nanocrystals. Two different impurity-impurity distances are considered in the codoped nanocrystals (dashed and solid lines, larger and smaller distances, respectively, see text). Red circles refer to $Si_{87}H_{76}$, blue squares to $Si_{147}H_{100}$. The lines are a guide for the eyes.

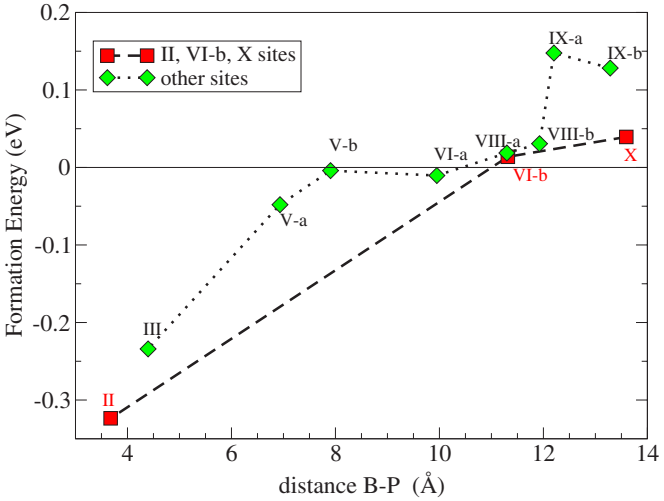

FIG. 8. (Color online) Formation energy as a function of the boron-phosphorus distance. Roman numbers label the positions of the P atom (see Fig. 4). The dotted and dashed lines connect two subsets of impurity sites, in which the surrounding surface Si atoms are bonded to the same number of passivating H atoms.

ergy gap as the gap between the impurity level (partially filled, considered as the HOMO) and the LUMO (which is empty). In these cases, the partially filled HOMO level is strongly localized either on the B or on the P impurity. For example, in the case of $Si_{86}BH_{76}$, the defect level is located just 0.28 eV above the valence band, reducing the above defined energy gap from 2.59 eV (the value for the undoped Si-nc) to 2.31 eV. In $Si_{86}PH_{76}$, the defect level is located just

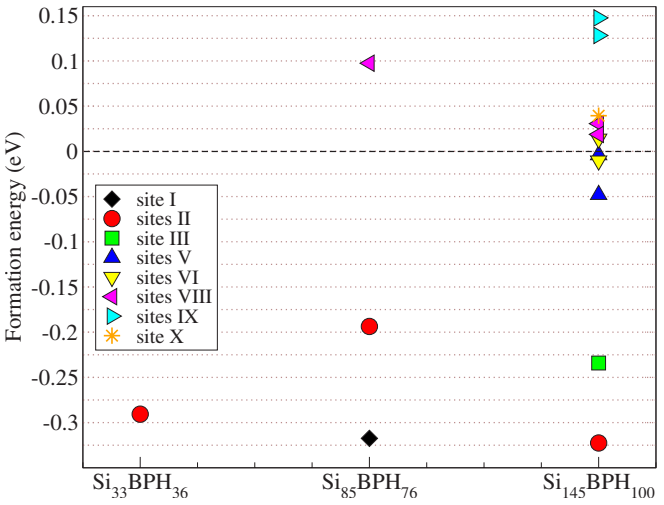

FIG. 9. (Color online) Formation energy as a function of Si-nc size and impurity-impurity distance. For the three different Si-nc, one has the following nanocrystal diameters (d) and impurity-impurity distances (D_{BP}): $Si_{33}BPH_{36}$, d=1.10 nm and D_{BP}=3.56 Å (site II); $Si_{85}BPH_{76}$, d=1.50 nm, and D_{BP}=2.00 Å (site I), D_{BP}=3.64 Å (site II), and D_{BP}=10.60 Å (site VIII); $Si_{145}BPH_{100}$, d=1.79 nm and D_{BP}=3.68 Å (site II), D_{BP}=4.40 Å (site III), D_{BP}=6.93 Å (site V-a), D_{BP}=7.91 Å (site V-b), D_{BP}=9.95 Å (site VI-a), D_{BP}=11.32 Å (site VI-b), D_{BP}=11.30 Å (site VIII-a), D_{BP}=11.93 Å (site VIII-b), D_{BP}=12.20 Å (site IX-a), D_{BP}=13.29 Å (site IX-b), and D_{BP}=13.59 Å (site X).

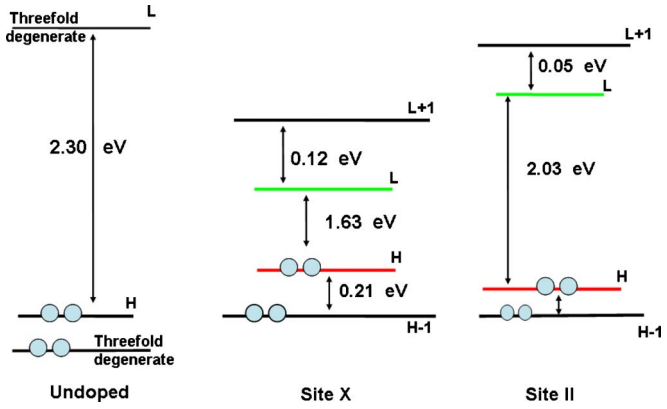

FIG. 10. (Color online) Calculated energy levels of the undoped $Si_{147}H_{100}$ (left panel), codoped $Si_{145}BPH_{100}$ with an impurity-impurity distance D_{BP}=13.29 Å (center panel), and codoped $Si_{145}BPH_{100}$ with an impurity-impurity distance D_{BP}=3.68 Å (right panel). The alignment has been done by locating at the same energy the fully occupied levels with the same type of localization. Site X and site II are referred to Fig. 4. H stands for HOMO, L for LUMO.

0.28 eV below the conduction band, so that the energy gap is only 0.28 eV.[19] It is interesting to note that the experimental substitutional donor binding energy for P in bulk Si is about 33 meV, while the experimental acceptor energy for B in Si is 45 meV,[38] showing how, in the case of nanocrystals, the combined effects of both quantum confinement and weak screening tend to "transform" shallow impurities in "deep" centers.[15,16,39,40]

The electronic properties of B- and P-codoped Si-nc are qualitatively and quantitatively different from those of either B- or P-single-doped Si-nc. Now the system is a semiconductor, and the presence of both impurities leads to a HOMO level that contains two electrons and to a HOMO-LUMO energy gap strongly lowered with respect to that of the corresponding undoped nanocrystals. Figure 10 shows the energy levels of $Si_{147}H_{100}$ and $Si_{145}BPH_{100}$, with the impurities located at two different distances. In one case, the impurities are placed at the largest possible distance (D_{BP}=13.29 Å), and in the other one, at the already discussed minimum distance (D_{BP}=3.68 Å) for this particular nanocrystal. From the figure, it is evident that when impurities are at the larger distance, E_G is strongly reduced with respect to the corresponding undoped value (E_G is lowered from 2.30 to 1.63 eV). On the contrary, when the impurities are close to each other, E_G enlarges (E_G=2.03 eV) although it still remains below the undoped case. We can think that when impurities are brought closer, the Coulomb interaction becomes stronger so that the energy gap becomes larger. Boron and phosphorus feel each other like B-P complexes, with a gap opening recalling the DFT-LDA calculated gaps of the boron phosphide bulk system: direct gap ($\Gamma \rightarrow \Gamma$) 3.3 eV, indirect gaps ($\Gamma \rightarrow X$) 2.2 eV, and ($\Gamma \rightarrow \Delta$) 1.2 eV, as described in Ref. 41.

These behaviors are corroborated by the calculated HOMO and LUMO wave functions. Figure 11 shows the square modulus contour plots of the HOMO and LUMO states of the two considered $Si_{145}BPH_{100}$ nanocrystals. The top panel shows the contour when the impurities are at a

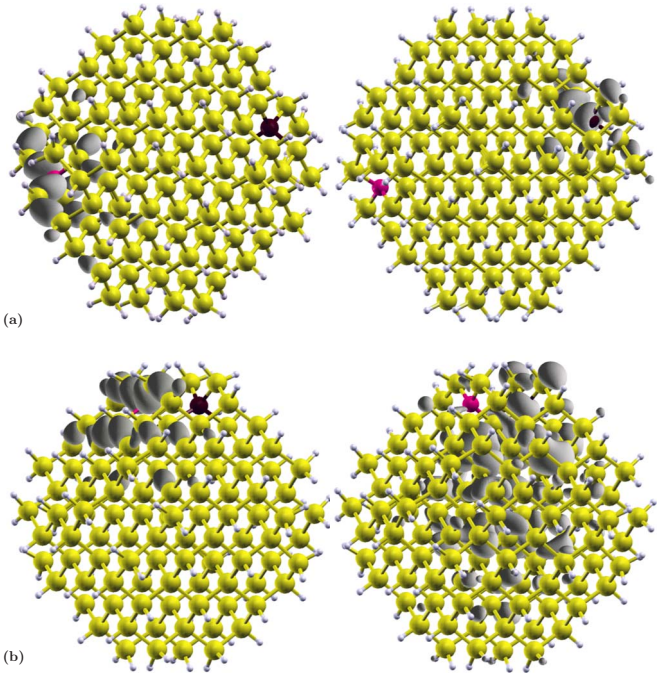

FIG. 11. (Color online) From the top to the bottom: the HOMO (left) and LUMO (right) square modulus contour plots calculated for $Si_{145}BPH_{100}$ (atom colors are the same as in Fig. 2). The impurities are located on opposite sides of the nanocrystal, at distance D_{BP}=13.29 Å (a), or as second neighbors, with an impurity-impurity distance D_{BP}=3.68 Å. The isosurfaces correspond to 10% of the maximum value.

large distance, while the bottom panel is that with the impurities at short distance. It clearly appears from these contours that in going from the case with well separated impurities to that with close impurities, the overlap between the HOMO, strongly centered on the boron atom, and the LUMO, mainly localized on the phosphorus atom, strongly increases.

Next we investigate how the electronic structure changes as a function of the impurity distance within the $Si_{145}BPH_{100}$ nanocrystal. In Fig. 12, we report the trend of the HOMO-LUMO energy gap with respect to the distance between impurities. It is seen that the mutual impurity distance affects not only the formation energy (see Sec. III B) but also the electronic structure. We observe that E_G decreases almost linearly with the increase of the impurity distance; moreover, also in this case, we can figure out the presence of two different trends related to the different surface regions experienced by the P atom in the sites II, VI-b, and X with respect to the other ones (see also Fig. 8 and related discussion). Figure 12 points out how, at least in principle, it is possible to tune E_G as a function of the impurity-impurity distance. It is easy to predict that for Si-nc larger than those considered here, it would be possible, by codoping, to obtain an energy gap even smaller than that of bulk Si.

The possibility of modulating the electronic properties of the codoped Si-nc is also evident if we keep the distance between the impurities constant and look at the dependence of the energy gap on the Si-nc size. Figure 13 shows, for three different nanocrystals where the impurities are placed as second neighbors, how the undoped nanocrystal energy

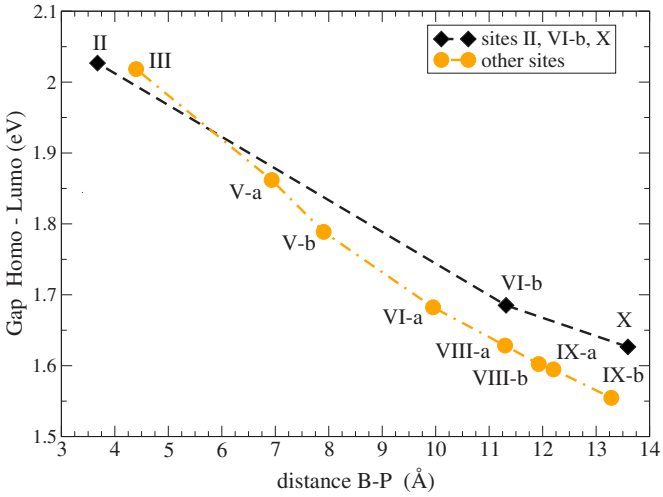

FIG. 12. (Color online) The HOMO-LUMO energy gap as a function of the distance between the B and P impurities within the $Si_{145}BPH_{100}$ nc. Roman numbers refer to the positions of the P atom (see Fig. 4). The dashed and dash-dotted lines connect the two subsets of impurity sites, in which the surrounding surface Si atoms are bonded to the same number of passivating H atoms.

gap is reduced in the presence of codoping (see also Table IV).

The same quantum confinement effect trend (i.e., larger gap for smaller nanocrystals) is observed for both the undoped and codoped cases. Moreover, the energy gap of the codoped Si-nc is shifted toward lower energies with respect to that of the undoped E_G; this shift is stronger for smaller nanocrystals. By playing with both the nanocrystal size and the distance between the impurities, new interesting routes may be opened for optoelectronic applications.

Looking at the energy gap trends in Figs. 12 and 13 and considering that in the codoped case Fujii *et al.*[13] found pho-

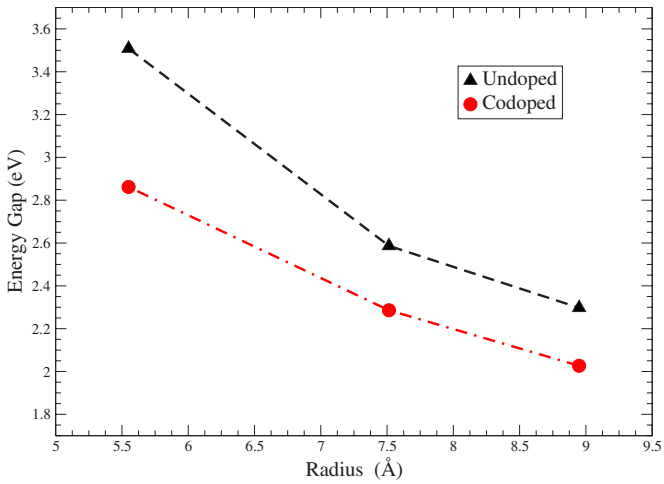

FIG. 13. (Color online) Comparison between energy gaps of the undoped (black triangles) and codoped (red circles) nanocrystals as a function of the nanocrystal radius. Impurities are located in the first shell below the surface, as second neighbors. The impurity-impurity distances are 3.56, 3.64, and 3.68 Å for $Si_{33}BPH_{36}$, $Si_{85}BPH_{76}$, and $Si_{145}BPH_{100}$, respectively. The lines are a guide for the eyes.

TABLE IV. HOMO-LUMO gap (E_G) for $Si_{35}H_{36}$, $Si_{87}H_{76}$, and $Si_{147}H_{100}$, and the corresponding codoped $Si_{33}BPH_{36}$, $Si_{85}BPH_{76}$, and $Si_{145}BPH_{100}$. Impurities are second neighbors. The impurity-impurity distances are 3.56, 3.64, and 3.68 Å for $Si_{33}BPH_{36}$, $Si_{85}BPH_{76}$, and $Si_{145}BPH_{100}$, respectively. d is the nanocrystal diameter.

Starting nc	d (nm)	E_G undoped (eV)	E_G codoped (eV)
$Si_{35}H_{36}$	1.10	3.51	2.86
$Si_{87}H_{76}$	1.50	2.59	2.29
$Si_{147}H_{100}$	1.79	2.30	2.03

toluminescence peaks centered in the 0.9–1.3 eV energy region, we may conclude that Si-nc playing a role in the experiment has dimensions of the order of a few nanometers. This conclusion is consistent with the experimental outcomes[13] that indicate an average nanocrystal diameter of about 5 nm.

D. Optical properties

The aim of this section is to investigate the mechanisms involved in the modification of the optical properties of codoped Si nanocrystals. We present absorption and emission spectra with a comparison between the independent particle–random phase approximation (IP-RPA) spectra and the many-body ones. These last ones are obtained within a GW-BSE approach that takes into account not only the self-energy correction and the local field effects but also the electron-hole interaction. All the calculations performed are not spin polarized. However, it should be noted that single-particle calculations for undoped Si-nc have been done by Franceschetti and Pantelides[30] within the local spin-density approximation, showing that the singlet-triplet splitting is significantly smaller than the Stokes shift. To understand the role of dimensionality and impurity distance and to show the importance of including many-body effects in the optical spectra, we are going to present first the result of a RPA independent particle optical response for various codoped nanocrystals different in dimensions and in impurity location (see Sec. III D 1). Next, we will present a complete study of a codoped Si-nc, where we go beyond the single-particle approach within the GW-BSE framework (see Sec. III D 2).

1. Absorption and emission spectra: Single-particle results

We first discuss the results related to the absorption spectra. Figure 14 shows a comparison between the undoped $Si_{87}H_{76}$ and the codoped $Si_{85}BPH_{76}$ IP-RPA absorption spectra. In this case, the impurities are located at a distance of 10.60 Å. The optical response is evaluated for the ground state relaxed geometry, computing the imaginary part of the dielectric function $\epsilon_2(\omega)$. It can be seen from Fig. 14 that new transitions arise below the absorption onset of the undoped Si-nc. In particular, we have found a shift of the absorption gap to lower energies with respect to the undoped case together with an enhancement of the intensities around

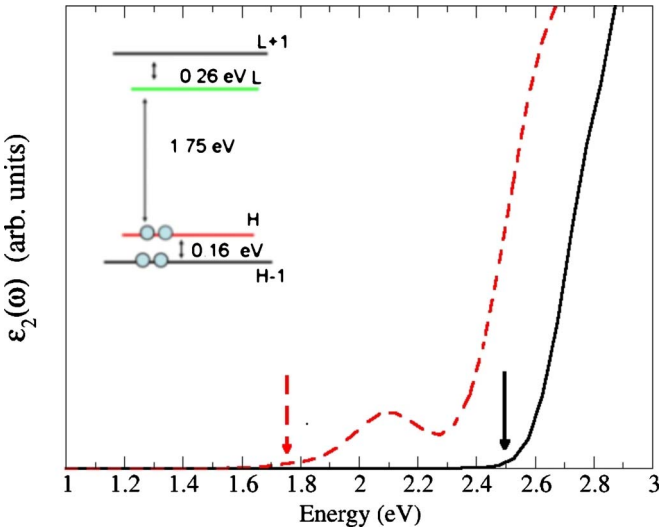

FIG. 14. (Color online) Comparison between the undoped $Si_{87}H_{76}$ (solid line) and codoped $Si_{85}BPH_{76}$ (dashed line) single-particle absorption spectra. The impurities are at a distance of 10.60 Å. Arrows indicate the energy gaps. The calculated energy levels for the codoped nanocrystal are shown in the inset. A Gaussian broadening of 0.1 eV has been applied. H stands for HOMO, L for LUMO.

2.0 eV. These new transitions are due to the presence of new HOMO and LUMO states localized on the impurities, as described in Sec. III C (see, for example, Fig. 11). The inset of Fig. 14 clarifies how the peak located in the 2.0–2.2 eV energy region is related to contributions that involve the HOMO-1, HOMO to LUMO, and LUMO+1 transitions; it should be noted that for all these levels, the wave functions are predominantly localized on the impurities. If we compare these results with those of a single-doped Si-nc,[42] we note that the presence of both impurities naturally suppresses all the absorption energy structures present in the infrared region (below 1 eV) of the single-doped spectra.

It is clear that, like the electronic properties, the optical properties also present a marked dependence on the nanocrystal dimension. To elucidate this point, we plot in Fig. 15 the single-particle absorption spectra of three different Si-nc, the $Si_{33}BPH_{36}$, $Si_{85}BPH_{76}$, and $Si_{145}BPH_{100}$, whose diameters are 1.10, 1.50, and 1.79 nm, respectively. In all three nanocrystals, the impurities are second neighbors. Two facts emerge from this figure. First of all, on increasing the nanocrystal size, the absorption gap is strongly reduced (see arrows in Fig. 15). Second, an increase of the Si-nc diameter (i.e., a decrease of the impurity weight with respect to the total number of atoms) results in a lowering of the intensity for the transitions that involve the impurities.

The role of the impurity distance on the optical response has been investigated following the same approach adopted for the electronic properties in Sec. III C. In Fig. 16, the single-particle absorption spectra of $Si_{145}BPH_{100}$ are reported with P impurity placed on sites II, III, IX, and X, respectively (see Fig. 4 for comparison). Here, we observe a shift of the absorption gap to lower energy on increasing the distance between the impurities (see arrows in Fig. 16). Moreover, the intensity is also affected by the impurity distance. Stronger

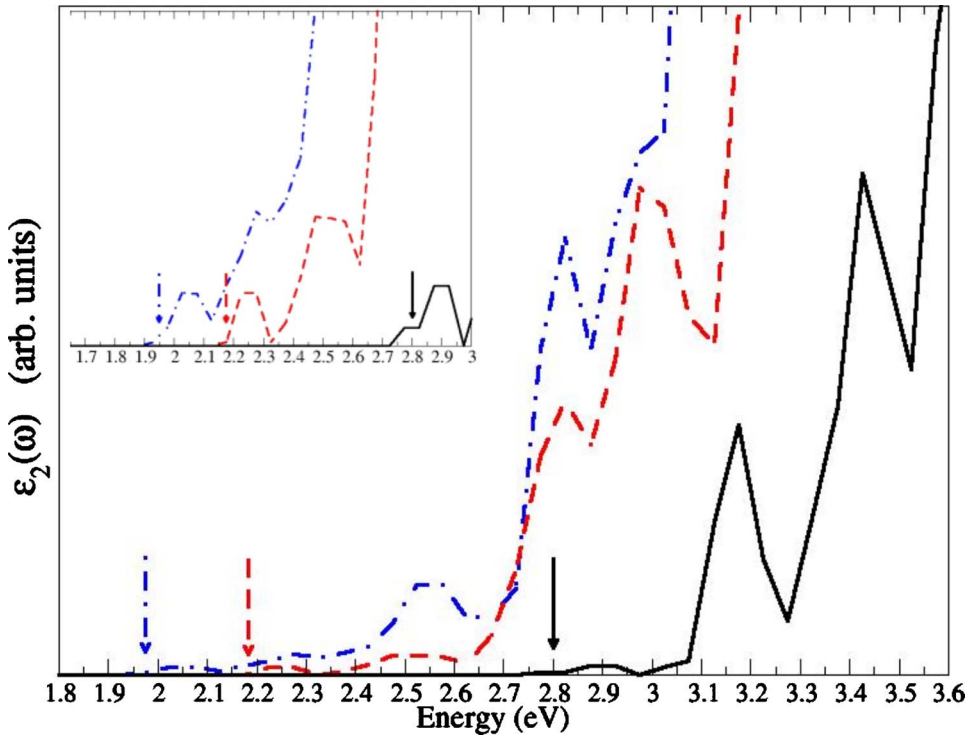

FIG. 15. (Color online) Single-particle absorption spectra of $Si_{33}BPH_{36}$ (black solid line), $Si_{85}BPH_{76}$ (red dashed line), and $Si_{145}BPH_{100}$ (dash-dotted blue line). In all cases, the impurities are second neighbors. The impurity-impurity distances are 3.56, 3.64, and 3.68 Å for $Si_{33}BPH_{36}$, $Si_{85}BPH_{76}$, and $Si_{145}BPH_{100}$, respectively. Arrows indicate the energy gaps. In the inset, is a zoomed view of the spectra onset. No Gaussian broadening has been applied.

transitions arise when the impurities are closer, whereas the intensity gets lower when the impurities are at larger distances; the optical transitions near the band edge (indicated by arrows in Fig. 16) exhibit weaker oscillator strengths.

Now we discuss the results for the emission spectra and for the Stokes shift between absorption and emission. The nanocrystal excitation has been studied considering the excited state as the electronic configuration in which the highest occupied single-particle state (HOMO) contains a hole (h), while the lowest unoccupied single-particle state (LUMO) contains the corresponding electron (e), thus simulating the creation of an electron-hole pair.[31,43–45] Initially, the system is in its ground state and the electronic excitation occurs with the atomic positions fixed in this configuration. After the excitation, due to the change in the charge density, relaxation occurs until the atoms reach a new minimum energy due to the presence of the electron-hole pair. The new atomic positions modify the electronic spectrum, implying that the levels involved in the emission process change. This model assumes that the relaxation under excitation is faster than the electron-hole recombination. The difference between the absorption and emission energies due to the different atomic positions represents the nanocrystal Stokes shift.[30,33,46]

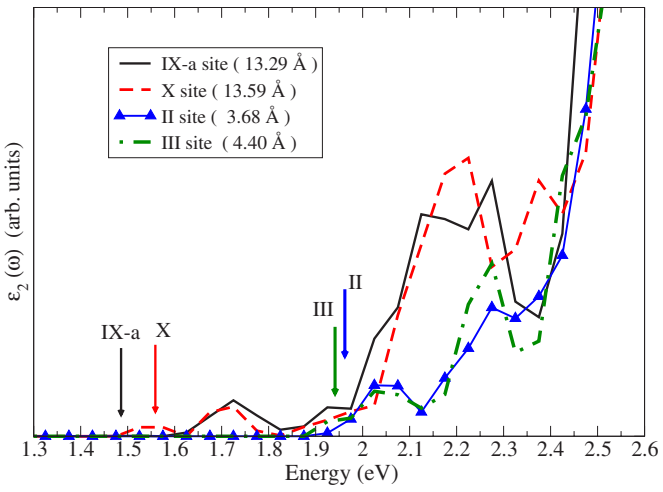

FIG. 16. (Color online) Single-particle absorption spectra of $Si_{145}BPH_{100}$ Si-nc with impurities placed at different distances (see the inset). Arrows indicate the energy gaps. Roman numbers refer to the sites occupied by the P atom with respect to the B one (see Fig. 4). No Gaussian broadening has been applied.

The calculations have been performed for two Si-nc of different sizes taking into account, in the larger Si-nc, the impurities located at different distances. As shown in Table V, both the absorption and emission HOMO-LUMO energies are affected by these two parameters. With regard to the first parameter, we note that the Stokes shift strongly depends on the size, showing a strong decrease upon increasing the diameter of the Si-nc. This is due to the fact that for larger nanocrystals, the excitation determines a minor distortion of the geometry. Concerning the second parameter, we see that the Stokes shift tends to slightly increase with B-P distance although this effect is small if compared with the lowering due to the increase of the Si-nc dimensions. The comparison

TABLE V. Absorption and emission energy gaps (and their difference, fifth row) calculated as HOMO-LUMO differences in the ground and excited relaxed geometry configurations, respectively. The results are obtained within the DFT single-particle approach. d is the nanocrystal diameter, D_{BP} is the distance between impurities, and Δ the calculated Stokes shift between absorption and emission energy gaps.

	$Si_{33}BPH_{36}$	$Si_{85}BPH_{76}$	
d (nm)	1.10	1.50	1.50
D_{BP} (Å)	3.56	2.00	10.60
Abs. (eV)	2.77	2.32	1.75
Ems. (eV)	1.78	2.20	1.36
Δ (eV)	0.99	0.12	0.39

between these results and the ones previously obtained for undoped clusters [0.92 eV for the $Si_{35}H_{36}$-nc (Ref. 26) and 0.22 eV for the $Si_{87}H_{76}$-nc (Ref. 31)] confirms that the Stokes shift is mainly determined by the nanocrystal size, but that, nevertheless, it depends slightly on the presence of the impurities and also on their mutual distance.

Looking at the single-particle optical spectra in Fig. 17, we note that the HOMO-LUMO transition in $Si_{85}BPH_{76}$ (1.75 eV, bottom panel) is almost dark when the two impurities are far apart and becomes, instead, allowed (2.32 eV,

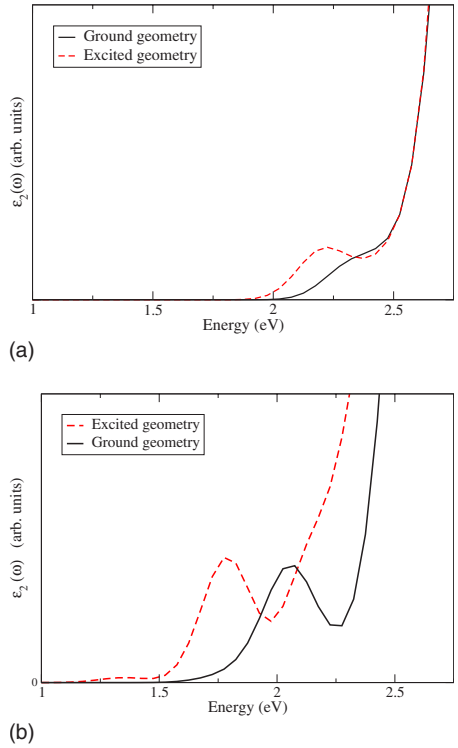

FIG. 17. (Color online) Single-particle imaginary part of the dielectric function for the codoped $Si_{85}BPH_{76}$ nanocrystal in the ground (black solid line) and excited (red dashed line) geometries. B and P atoms are at the smallest possible distance (2.00 Å, top panel) or at the largest possible distance (10.60 Å, bottom panel) for this nanocrystal. A Gaussian broadening of 0.1 eV has been applied.

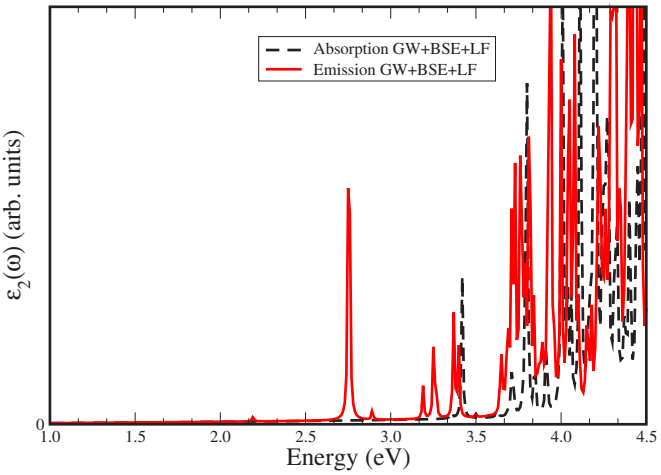

FIG. 18. (Color online) Absorption (black dashed line) and emission (red solid line) many-body spectra of $Si_{33}BPH_{36}$.

top panel) when their distance decreases. As discussed before, this oscillator strength enhancement is a consequence of the character of the HOMO and LUMO states in the two cases. The emission (red-dashed lines in Fig. 17) spectra are redshifted with respect to the absorption (black solid lines in Fig. 17). This redshift is a consequence of the geometry relaxation in the excited state due to the excess energy necessary to promote an electron in the LUMO level. The dependence of the emission spectra both on the nanocrystals' size (see Table V and Fig. 15) and on the impurities' positions (see Figs. 16 and 17) reveals, once more, the possibility of tuning the optical response of silicon nanocrystals.

2. Absorption and emission spectra: Many-body effects

In order to give a complete description, within the many-body framework, of the codoped Si-nc response to an optical excitation, we consider both the self-energy corrections by means of the GW method[47] to obtain the quasiparticle energies and the excitonic effects through the solution of the Bethe-Salpeter equation. The effect of local fields is also included to take into account the inhomogeneity of the systems.

Since the GW-BSE calculation[48] is very computationally demanding, we have only considered the smaller codoped nanocrystal $Si_{33}BPH_{36}$ (see Fig. 2). In this particular cluster, we found that local field effects are, although not negligible, of minor importance with respect to GW and excitonic effects. It is, however, essential to include *all* of them (LF and many-body) in order to get the final converged spectrum shown in Fig. 18. In order to carry out emission spectra calculations, we use the excited state geometry and the ground state electronic configuration. As already noted before, in this case, $\epsilon_2(\omega)$ corresponds to an absorption spectrum in a new structural geometry. In other words, we consider the emission as the time reversal of the absorption.[33,34] Thus, the electron-hole interaction is considered here also in the emission geometry. The heavy GW-BSE calculation is made considering a large fcc supercell with a 50 a.u. lattice parameter. The correlation part of the self-energy Σ_c has

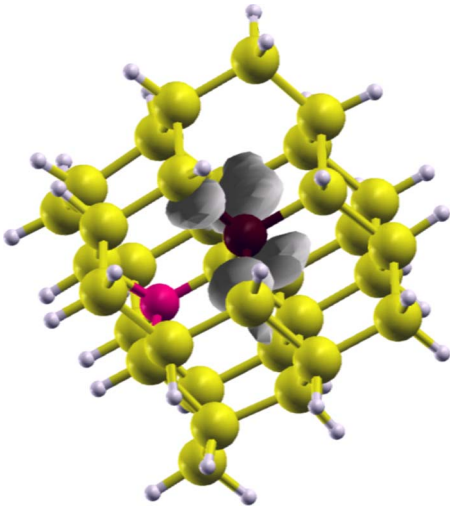

FIG. 19. (Color online) Excitonic wave function of $Si_{33}BPH_{36}$ (atom colors as in Fig. 2). The gray isosurface represents the probability distribution $|\psi_{exc}(r_e,r_h)|^2$ of the electron, with the hole fixed on the B impurity.

been calculated using 10 081 plane waves, while 49 805 plane waves have been used for the exchange part Σ_x. Then, the full excitonic Hamiltonian is diagonalized considering more than 8000 transitions.

Figure 18 shows the calculated absorption and emission spectra, fully including the many-body effects. The electron-hole interaction yields significant variations with respect to the single-particle spectra (see Fig. 17 for a comparison), with an important transfer of the oscillator strength to the low energy side. Moreover, in the emission spectrum, the rich structure of states characterized, in the low energy side, by the presence of excitons with largely different oscillator strengths determines excitonic gaps well below the optical absorption onset. Thus the calculated emission spectrum is redshifted to lower energy with respect to the absorption spectrum. This energy difference between emission and absorption, the Stokes shift, can be traced back to the relaxation of the Si-nc after the excitation process.

The important features that appear in the emission many-body spectra are related to the presence of both B and P impurities, as shown by Fig. 19, which gives the real-space probability distribution $|\psi_{exc}(r_e,r_h)|^2$ for the bound exciton as a function of the electron position r_e when the hole is fixed in a given r_h position. In this case, the hole is fixed on the boron atom and we see that the bound exciton is mainly localized around the phosphorus atom.

From Table VI, it can be seen that the single-particle DFT results strongly underestimate the absorption and emission edges with respect to the GW+BSE calculation, in which the excitonic effects are taken exactly into account. This means that, in this case, the cancellation between GW gap opening (which gives the electronic gap) and BSE gap shrinking (which originates the excitonic gap) is only partial.[49]

The difference between the GW electronic gap and the GW+BSE optical excitonic gap gives the exciton binding energy E_b. We note the presence of exciton binding energies as big as 2.2 eV, which are very large if compared with bulk Si ($\sim$15 meV) or with carbon nanotubes,[50,51] where $E_b \sim 1$ eV, but are similar to those calculated for undoped Si-nc (Ref. 33) of similar size and for small Si and Ge nanowires.[52,53]

TABLE VI. Absorption and emission energies calculated as HOMO-LUMO energy difference within the single-particle DFT, the many-body GW, and the GW+BSE approaches. Δ is the calculated Stokes shift between absorption and emission energy gaps. The 2.20 eV energy corresponds to an almost dark transition.

$Si_{33}BPH_{36}$	DFT	GW	GW+BSE
Abs. (eV)	2.80	5.52	3.35
Ems. (eV)	1.79	4.37	2.20
Δ (eV)	1.01	1.15	1.15

The differences between full many-body calculations and single-particle results are 0.55 and 0.41 eV for absorption and emission energy gaps, respectively, and 0.14 eV between the two Stokes shifts. It is interesting to note that the HOMO-LUMO transition in the emission spectrum at 2.20 eV is almost dark, while an important excitonic peak is evident at about 2.75 eV (see Fig. 18), again redshifted with respect to the first absorption peak. As expected, what comes out is the importance of fully taking into account the many-body aspect of the problem in order to overcome the limits of the single-particle approach.

IV. CONCLUSIONS

The structural, electronic, and optical properties of Si nanocrystals codoped with B and P impurities have been studied also beyond the single-particle approach. We have considered Si-nc of different sizes and with the impurities located at different distances. We show that codoping is always energetically favored with respect to simple B or P doping and that the two impurities tend to occupy nearest neighbor sites near the surface rather than other positions inside the nanocrystal itself. Our results demonstrate that the codoped nanocrystals present valence and conduction band-edge states which are localized on the two impurities, respectively, and band gaps always lower in energy with respect to that of undoped Si nanocrystals. Besides, the electronic properties show a dependence on both nanocrystal size and impurity-impurity distance. The impurity located band-edge states originate absorption thresholds in the visible region, which are shifted lower in energy with respect to the undoped case. Moreover, the emission spectra show a Stokes shift with respect to the absorption, which is due to the structural relaxation after the creation of the electron-hole pair. Our results make evident the presence of electronic quasi-direct optical transitions between donor and acceptor states that can help in understanding the experimental outcomes and make it possible to engineer the absorption and emission properties of Si nanocrystals.

ACKNOWLEDGMENTS

We acknowledge the support of the MIUR PRIN (2005) Italy, of the CNR-CNISM "Progetto Innesco" of the CRUI Vigoni Project (2005-2006) Italy-Germany, and of EU Nanoquanta Network of Excellence (NMP4-CT-2004-500198). All the calculations were performed at CINECA-Bologna ("Iniziativa Calcolo Parallelo del CNR-INFM"), CICAIA-Modena, and "Campus Computational Grid"-Università di Napoli "Federico II."

[1] S. Ossicini, L. Pavesi, and F. Priolo, *Light Emitting Silicon for Microphotonics* (Springer, Berlin, 2003).
[2] V. N. Borisenko and S. Ossicini, *What is What in the Nanoworld* (Wiley-VCH, Weinheim, 2004).
[3] O. Bisi, S. Ossicini, and L. Pavesi, Surf. Sci. Rep. **38**, 1 (2000).
[4] B. Gelloz, A. Kojima, and N. Koshida, Appl. Phys. Lett. **87**, 031107 (2005).
[5] L. Pavesi, L. Dal Negro, C. Mazzoleni, G. Franzó, and F. Priolo, Nature (London) **408**, 440 (2000).
[6] L. Dal Negro, M. Cazzanelli, L. Pavesi, S. Ossicini, D. Pacifici, G. Franzó, and F. Priolo, Appl. Phys. Lett. **82**, 4636 (2003).
[7] J. Ruan, P. M. Fauchet, L. Dal Negro, M. Cazzanelli, and L. Pavesi, Appl. Phys. Lett. **83**, 5479 (2003).
[8] M. Cazzanelli, D. Kovalev, L. Dal Negro, Z. Gaburro, and L. Pavesi, Phys. Rev. Lett. **93**, 207402 (2004).
[9] K. Luterová, K. Dohnalová, V. Šervček, I. Pelant, J.-P. Likforman, O. Crégut, P. Gilliot, and B. Hönerlage, Appl. Phys. Lett. **84**, 3280 (2004).
[10] *Properties of Porous Silicon*, edited by L. T. Canham (INSPEC, London, 1997).
[11] C. Delerue, G. Allan, and M. Lannoo, Phys. Rev. B **64**, 193402 (2001).
[12] M. Fujii, Y. Yamaguchi, Y. Takase, K. Ninomiya, and S. Hayashi, Appl. Phys. Lett. **87**, 211919 (2005).
[13] M. Fujii, K. Toshikiyo, Y. Takase, Y. Yamaguchi, and S. Hayashi, J. Appl. Phys. **94**, 1990 (2003).
[14] M. Fujii, Y. Yamaguchi, Y. Takase, K. Ninomiya, and S. Hayashi, Appl. Phys. Lett. **85**, 1158 (2004).
[15] D. V. Melnikov and J. R. Chelikowsky, Phys. Rev. Lett. **92**, 046802 (2004).
[16] G. Cantele, E. Degoli, E. Luppi, R. Magri, D. Ninno, G. Iadonisi, and S. Ossicini, Phys. Rev. B **72**, 113303 (2005).
[17] Z. Zhou, M. L. Steigerwald, R. A. Friesner, L. Brus, and M. S. Hybertsen, Phys. Rev. B **71**, 245308 (2005).
[18] M. V. Fernández-Serra, C. Adessi, and X. Blase, Phys. Rev. Lett. **96**, 166805 (2006).
[19] S. Ossicini, E. Degoli, F. Iori, E. Luppi, R. Magri, G. Cantele, F. Trani, and D. Ninno, Appl. Phys. Lett. **87**, 173120 (2005).
[20] S. Ossicini, F. Iori, E. Degoli, E. Luppi, R. Magri, R. Poli, G. Cantele, F. Trani, and D. Ninno, IEEE J. Sel. Top. Quantum Electron. **12**, 1585 (2006).
[21] S. Baroni, A. Dal Corso, S. de Gironcoli, P. Giannozzi, C. Cavazzoni, G. Ballabio, S. Scandolo, G. Chiarotti, P. Focher, A. Pasquarello, K. Laasonen, A. Trave, R. Car, N. Marzari, and A. Kokalj, http://www.pwscf.org/
[22] L. C. Ciacchi and M. C. Payne, Phys. Rev. Lett. **95**, 196101 (2005).
[23] E. Garrone, F. Geobaldo, P. Rivolo, G. Amato, L. Boarino, M. Chiesa, E. Giamello, R. Gobetto, P. Ugliengo, and A. Vitale, Adv. Mater. (Weinheim, Ger.) **17**, 528 (2005).
[24] D. Vanderbilt, Phys. Rev. B **41**, R7892 (1990).
[25] We have checked that the use of Vanderbilt or norm-conserving pseudopotentials does not affect the calculated structural properties of the Si-nc.
[26] E. Degoli, G. Cantele, E. Luppi, R. Magri, D. Ninno, O. Bisi, and S. Ossicini, Phys. Rev. B **69**, 155411 (2004).
[27] S. B. Zhang and J. E. Northrup, Phys. Rev. Lett. **67**, 2339 (1991).
[28] X. Luo, S. B. Zhang, and S.-H. Wei, Phys. Rev. Lett. **90**, 026103 (2003).
[29] L. G. Wang and A. Zunger, Phys. Rev. B **66**, 161202(R) (2002).
[30] A. Franceschetti and S. T. Pantelides, Phys. Rev. B **68**, 033313 (2003).
[31] A. Puzder, A. J. Williamson, J. C. Grossman, and G. Galli, J. Am. Chem. Soc. **125**, 2786 (2003).
[32] G. Onida, L. Reining, and A. Rubio, Rev. Mod. Phys. **74**, 601 (2002), and references therein.
[33] E. Luppi, F. Iori, R. Magri, O. Pulci, S. Ossicini, E. Degoli, and V. Olevano, Phys. Rev. B **75**, 033303 (2007).
[34] F. Bassani and G. Pastori Parravicini, *Electronic States and Optical Transitions in Solids* (Pergamon, New York, 1975).
[35] W. Van Roosbroeck and W. Shockley, Phys. Rev. **94**, 1558 (1954).
[36] L. Hedin, Phys. Rev. **139**, A796 (1965).
[37] F. Trani, D. Ninno, and G. Iadonisi, Phys. Rev. B **75**, 033312 (2007).
[38] P. Y. Yu and M. Cardona, *Fundamentals of Semiconductors* (Springer, Berlin, 2001).
[39] D. Ninno, F. Trani, G. Cantele, K. Hameeuw, G. Iadonisi, E. Degoli, and S. Ossicini, Europhys. Lett. **74**, 519 (2006).
[40] F. Trani, D. Ninno, G. Cantele, G. Iadonisi, K. Hameeuw, E. Degoli, and S. Ossicini, Phys. Rev. B **73**, 245430 (2006).
[41] R. M. Wentzcovitch, K. J. Chang, and M. L. Cohen, Phys. Rev. B **34**, 1071 (1986).
[42] F. Iori, E. Degoli, E. Luppi, R. Magri, I. Marri, G. Cantele, D. Ninno, F. Trani, and S. Ossicini, J. Lumin. **121**, 335 (2006).
[43] R. W. Godby and I. D. White, Phys. Rev. Lett. **80**, 3161 (1998).
[44] A. Franceschetti, L. W. Wang, and A. Zunger, Phys. Rev. Lett. **83**, 1269 (1999).
[45] H.-C. Weissker, J. Furthmüller, and F. Bechstedt, Phys. Rev. Lett. **90**, 085501 (2003).
[46] We note that the difference that arises in calculating the energy gap using the HOMO-LUMO gap or the Δ-SCF method strongly shrinks as the dimension of the nanocrystal increases (Refs. 26 and 31).
[47] We have used the non-self-consistent G_0W_0 approach within the RPA plasmon pole approximation. We use a plane-wave–frequency space code.
[48] V. Olevano, EXC code, http://www.bethe-salpeter.org
[49] C. Delerue, M. Lannoo, and G. Allan, Phys. Rev. Lett. **84**, 2457 (2000).

[50] C. D. Spataru, S. Ismail-Beigi, L. X. Benedict, and S. G. Louie, Phys. Rev. Lett. **92**, 077402 (2004).
[51] E. Chang, G. Bussi, A. Ruini, and E. Molinari, Phys. Rev. Lett. **92**, 196401 (2004).
[52] M. Bruno, M. Palummo, R. Del Sole, V. Olevano, A. N. Kholod, and S. Ossicini, Phys. Rev. B **72**, 153310 (2005).
[53] M. Bruno, M. Palummo, A. Marini, R. Del Sole, and S. Ossicini, Phys. Rev. Lett. **98**, 036807 (2007).